JOURNAL OF SPACECRAFT AND ROCKETS
Vol. 29, No. 5, September-October 1992

Numerical Simulation of High-Speed Flows About Waveriders with Sharp Leading Edges

Kevin D. Jones* and F. Carroll Dougherty†
University of Colorado, Boulder, Colorado 80309

A procedure for the numerical simulation of stagnation-free, inviscid, supersonic and hypersonic flows about geometries with sharp leading edges has been developed. Specialized grid generation techniques, an algebraic solution-adaptive grid scheme, and a modified flow solving method are discussed. Results for several waverider geometries are presented and compared with exact solutions, other numerical solutions, and experimental results. The results demonstrate the ability of this procedure to produce stagnation-free Euler solutions about sharp-edged configurations and to capture the physics of the flow in these regions accurately.

Nomenclature

a_1, a_2, a_3	= vector components of A in three space
b_1, b_2, b_3	= vector components of B in three space
$\lvert C \rvert$	= magnitude of vector C
C_D	= drag coefficient
C_L	= lift coefficient
c_1, c_2, c_3	= vector components of C in three space
$\lvert D \rvert$	= magnitude of vector D
d_1, d_2, d_3	= vector components of D in three space
e	= energy
F	= scalar on which grid adaptation is based
$\hat{i}, \hat{j}, \hat{k}$	= unit vectors in Cartesian coordinates
L/D	= lift over drag
M	= Mach number
p	= pressure
S_1	= arclength coordinate along a grid line
S_2	= arclength coordinate along $F(S_1)$
$x_1(j,k)$	= x Cartesian coordinate of $P(j,k)$
$x_2(j,k)$	= y Cartesian coordinate of $P(j,k)$
$x_3(j,k)$	= z Cartesian coordinate of $P(j,k)$
ζ	= radial curvilinear coordinate
η	= circumferential curvilinear coordinate
ξ	= axial curvilinear coordinate
ρ	= density
$\rho u, \rho v, \rho w$	= momentum in the x, y, and z Cartesian directions

I. Introduction

IN recent years concepts such as the National Aero-Space Plane (NASP) have led to renewed interest in the design of efficient supersonic and hypersonic configurations. In the search for high-speed performance, an old idea, the waverider, has regained popularity. Once thought to represent interesting but purely academic analytic solutions to the Euler equations, classes of waveriders have turned out to be competitive designs at hypersonic speeds.

Waveriders were first conceptualized in 1959 by Nonweiler[1] as a tool for the analytic study of heat conduction in sharp leading edges as applied to atmospheric re-entry vehicles. Nonweiler's classic inverted-V and inverted-W wing waveriders were inversely designed by tracing a stream surface through the known flowfields behind planar oblique shock waves. In inviscid theory the stream surface could be replaced by a solid surface, thus defining the lower surface of the waverider. In 1963 Jones[2] introduced an extension of this method for the flowfields over nonlifting circular cones. In the following years many other scientists, too numerous to list here, have contributed to the waverider design effort.

This type of inverse design approach offers several advantages over direct design methods. At high supersonic speeds it is frequently desirable to control the position of the shock wave with respect to the engine inlet lip. By inversely creating a waverider surface that will reproduce a prescribed shock wave, this becomes a simple task. In addition, the engines' performances will be greatly influenced by the flow properties entering the inlet. Since the choice of the shock shape defines the flow qualities behind the shock, favorable flow properties can be designed into the aircraft's flowfield.

An ongoing research project by the present authors and several colleagues has supported the development of two such inverse design algorithms and a number of conventional computational fluid dynamics (CFD) tools for the design, optimization, and evaluation of waverider geometries.[3] Computational tools for the direct Euler simulation of the flowfields about these waverider topologies were required as a means of validating the inverse design methods. To duplicate the inverse design results, the Euler simulations had to be able to compute shock strength and location accurately, including shock attachment at sharp leading edges. To facilitate this, a means of producing stagnation-free flows about sharp leading edges was needed.

The numerical procedures developed for the grid-generation, solution-based grid adaptation, and Euler analysis of the waverider geometries are discussed in Sec. II, and Sec. III presents results for three waverider test cases and comparisons with exact theory, other numerical results, and experimental data.

II. Numerical Approach

The numerical simulation of fluid flows involves significant efforts in both grid generation and flow solving. The two tasks can often be handled independently, but the accuracy of the resultant solutions is generally dependent on both. The grid generation, solution adaption, and flow solving methods utilized in this study are discussed in this section.

Grid Generation

Well-constructed grids are crucial to the accuracy and stability of the solution to a finite difference problem. The

---

Presented as Paper 90-3065 at the AIAA 8th Applied Aerodynamics Conference, Portland, OR, Aug. 20-22, 1990; received June 8, 1991; revision received Jan. 20, 1992; accepted for publication March 2, 1992.

*Graduate Research Assistant, Department of Aerospace Engineering Sciences, College of Engineering, Campus Box 429. Student Member AIAA.

†Adjunct Professor, Department of Aerospace Engineering Sciences, College of Engineering. Member AIAA.

generation of suitable grids can often be a considerable task, depending on the geometry of the given problem. The waverider topologies provide several technical gridding difficulties primarily due to the configurations' sharp leading edges. Many grid generators create highly skewed or overlapping grid cells in the vicinity of sharp edges.

Several existing routines, GRAPE3D, GRID3D, and GRIDF, were considered, but each failed in at least one area. Neither GRAPE3D, a NASA Ames elliptic grid generator, nor GRID3D, an algebraic trans-finite interpolation (TFI) solver, was able to handle the sharp leading edges adequately. Both codes produced highly skewed or overlapping grid cells near the sharp edge. A pseudo three-dimensional code, GRIDF, was able to handle sharp edges, but its two-dimensional TFI algorithm required $\xi = \text{const}$ grid planes to lie in planes of constant x value and provided insufficient continuity between adjacent grid planes, resulting in highly skewed grid cells near the nose of the configurations. All three of these codes produced unsuitable outer boundary shapes, placing many grid points far from the affected flow region.

Due to the lack of success with these existing codes, a specialized grid generator, HYGRID, was developed for the waverider geometries. The difficulty that many grid generators have at sharp edges originates from their computation of the surface normals. Analytically the normal at a point P is defined as the vector product of two nonparallel vectors tangent to the surface at P as illustrated in Fig. 1a. Numerically, this is typically approximated with central finite differences as follows:

$$a_i = x_i(j+1,k) - x_i(j-1,k), \qquad i = 1,2,3 \tag{1a}$$

$$b_i = x_i(j,k+1) - x_i(j,k-1), \qquad i = 1,2,3 \tag{1b}$$

Vectors $\boldsymbol{A}$ and $\boldsymbol{B}$ are defined from Eqs. (1a) and (1b) as

$$\boldsymbol{A} = \hat{i}a_1 + \hat{j}a_2 + \hat{k}a_3 \tag{2a}$$

$$\boldsymbol{B} = \hat{i}b_1 + \hat{j}b_2 + \hat{k}b_3 \tag{2b}$$

The normal components are given by

$$\begin{aligned} n_1 &= a_2b_3 - a_3b_2 \\ n_2 &= a_3b_1 - a_1b_3 \\ n_3 &= a_1b_2 - a_2b_1 \end{aligned} \tag{3}$$

with the normal given by

$$\boldsymbol{N} = \hat{i}n_1 + \hat{j}n_2 + \hat{k}n_3 \tag{4}$$

This approach, illustrated in Fig. 1b, is accurate for slightly curved surfaces or with evenly spaced grid points. However, at sharp edges the accuracy of Eqs. (2a) and (2b) becomes strongly dependent on the grid spacing. Figures 2a and 2b illustrate the normals computed by Eq. (4) at a two-dimensional sharp edge with evenly and unevenly spaced grid points, respectively, using Eqs. (2a) and (2b) to approximate the tangents. It may not always be possible or desirable to have evenly distributed points, so an alternate method was developed to alleviate this problem. In the new scheme, illustrated two-dimensionally in Fig. 3, vectors $\boldsymbol{C}$ and $\boldsymbol{D}$ are defined with the directions of the line segments OP and PQ, respectively, but each with a length of 1. The vector $\boldsymbol{A}$ is then the vector sum of $\boldsymbol{C}$ and $\boldsymbol{D}$. Numerically the vector components of $\boldsymbol{C}$ and $\boldsymbol{D}$ are given by

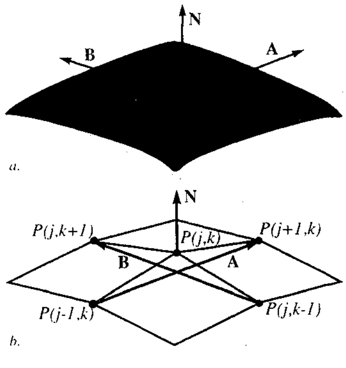

Fig. 1 Surface normal definition, a) analytical approach, b) numerical approach.

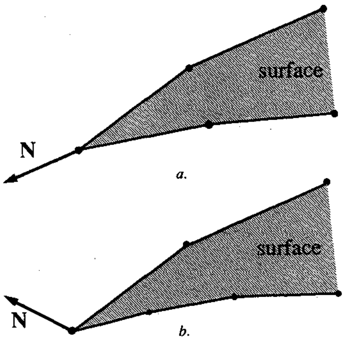

Fig. 2 Typical normal computation at a sharp edge with grid points distributed a) evenly and b) unevenly.

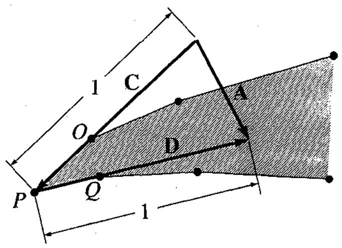

Fig. 3 Modified normal computation for sharp edges.

$$\begin{aligned} c_i &= x_i(j,k) - x_i(j-1,k), \qquad i = 1,2,3 \\ d_i &= x_i(j+1,k) - x_i(j,k), \qquad i = 1,2,3 \end{aligned} \tag{5}$$

The magnitudes of $\boldsymbol{C}$ and $\boldsymbol{D}$ are given by

$$\begin{aligned} |\boldsymbol{C}| &= \sqrt{c_1^2 + c_2^2 + c_3^2} \\ |\boldsymbol{D}| &= \sqrt{d_1^2 + d_2^2 + d_3^2} \end{aligned} \tag{6}$$

such that the normalized components are given by

$$\begin{aligned} c_i' &= \frac{c_i}{|\boldsymbol{C}|}, \qquad i = 1,2,3 \\ d_i' &= \frac{d_i}{|\boldsymbol{D}|}, \qquad i = 1,2,3 \end{aligned} \tag{7}$$

The vector components of $\boldsymbol{A}$ are then

$$a_i = c_i' + d_i', \qquad i = 1,2,3 \tag{8}$$

such that

$$\boldsymbol{A} = \hat{i}a_1 + \hat{j}a_2 + \hat{k}a_3 \tag{9}$$

The vector $\boldsymbol{B}$ is defined similarly. The normal is then computed with Eq. (4) using the vector components of $\boldsymbol{A}$ found from Eq. (8). This method is obviously more computationally expensive and is, consequently, only applied at predefined sharp edges.

For the waverider geometries considered here, the sharp leading edge is placed close to the outer boundary. To further reduce grid irregularities in this area, the grid lines extending from the sharp edge are mapped straight out to the outer boundary in the direction of the computed normals as illustrated in Fig. 4.

HYGRID utilizes a three-dimensional TFI algorithm developed by Rizzi and Eriksson.[4] In the current form, first-through fourth-order exponential or polynomial blending functions are available providing varying degrees of grid orthogonality control near the surface. Grid spacing at the surface is explicitly specified at several surface points and bilinearly interpolated over the rest of the surface. Grid clustering between the surface and the outer boundary is computed as a geometric progression. Outer boundary shapes to efficiently encapsulate the affected flow regions are generated, reducing the number of grid points in the undisturbed flow.

Solution-Adaptive Gridding

To increase shock resolution with a minimum number of grid points, a solution-adaptive grid technique is employed. The adaptive scheme uses an algebraic procedure to recluster points in only one computational direction based on the gradients of a specified scalar function. Reclustering in only one computational direction simplifies the procedure significantly and helps to preserve grid quality near the sharp edges.

The algorithm is briefly summarized as follows. The specified scalar F is given as a function of the arclength S_1 along the grid line. A function S_2 is defined as the arclength along the curve given by $F(S_1)$. A linear spline is formed defining S_1 as a function of S_2. A new, linear distribution of points on S_2 automatically clusters points along S_1 at high gradients of F. Clustering at the wall is preserved by turning off the adaptation in a specified region, and by modifying the linear distribution along S_2, the unadapted and adapted regions can be smoothly blended together. The new distribution along S_1 is incorporated into a three-dimensional grid line by forming cubic splines defining x, y, z, and the five scalars, ρ, ρu, ρv, ρw, and e, as functions of S_1, and then interpolating the new coordinate and scalar values for the reclustered arclength distribution from the spline. The extent of the clustering can be controlled several ways. The magnitude of the scalar F can be scaled with respect to the arclength S_1, effectively reducing the magnitude of gradients, or a weighted averaging of the original and reclustered distribution can be used to relax the clustering.

In the flowfields of this study most of the strong gradients are roughly aligned with the ζ grid lines, that is, the radial grid lines extending from the surface to the outer boundary. Consequently, that is the computational direction in which the grids are reclustered. Adaptation is based on density ρ and is only performed once or twice during convergence. To expedite the convergence, the first adaptation is not performed until the shock has formed and moved to approximately the expected position. Since there are no high-density gradients at the wall in the Euler solutions, the wall clustering is fixed to adequately resolve surface pressure. The magnitude of the clustering is controlled globally by scaling the values of the scalar function, and to avoid difficulties at the sharp edge, the magnitude is also controlled locally by averaging the unadapted and adapted distributions in the vicinity of the leading edge. A typical solution with an adapted grid is shown in Fig. 5.

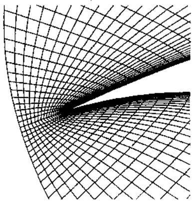

Fig. 4 Grid detail near a sharp edge.

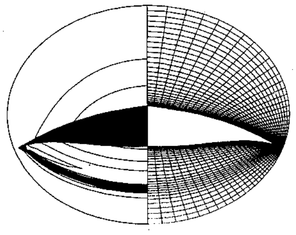

Fig. 5 Solution-based grid adaptation.

Flow Solving

Two finite difference codes, ARC3D[5] and F3D,[6] were considered for this project because of their ready availability and the present authors' familiarity with the codes. Both codes apply the alternating direction implicit (ADI) algorithm of Beam and Warming and solve either the Euler or thin-layer Navier-Stokes equations in generalized, body-fitting coordinates for steady or time-dependent simulations. F3D, however, utilizes an upwinding or flux-split scheme in the streamwise direction, providing a more efficient algorithm and greater stability at high Mach numbers. F3D has previously been used successfully for a number of studies at high Mach numbers, and consequently it was selected for this study.

Several boundary condition modifications were necessary for this application. All of the configurations considered were symmetric; hence, to minimize the computational effort, a symmetry boundary condition was used. In its original form, F3D provided symmetry for the conserved variables but not for the fourth-order dissipative terms. On several test cases this resulted in every-other-point oscillations in the solution along the symmetry plane that eventually caused the solutions to diverge.

A second difficulty originated from the sharp leading edges. Duplication of the inverse design results required the capturing of attached shock waves with stagnation-free flows. From a purely theoretical point of view, the velocity can be defined on the upper and lower surfaces near the sharp edge. However, these two velocities will, in general, have different magnitudes and directions, and hence a single grid point cannot accurately model the flow physics. Similarly, the other flow parameters, such as ρ and e, will have multiple values at this single point as well. A so-called "sharp" boundary condition was developed to handle this "singularity" in the velocity field caused by the sharp edge.

Since the flow cannot be modeled accurately using a single grid point at the sharp edge, two possible options are immediately apparent. Either two coincident points can be stored for the leading edge, one for the upper surface and one for the lower surface, or no points can be used at the leading edge. Using two coincident points presents additional numerical difficulties. For instance, the accuracy of the finite difference formulas is questionable, since the aspect ratio of adjacent grid cells will be infinite. However, by placing no grid points at the leading edge there is the question of whether or not the code will know where the leading edge is supposed to be. Although both methods have advantages and disadvantages, the second method was selected for this study. The feasibility of the first method has not been tested, and may provide an interesting extension of this work.

To achieve this "no-point" leading edge, two tasks are performed. First, the surface grid is modified such that there are no points on the aircraft's leading edge. This is done by moving the grid points that lie on the "physical" leading edge out into the flowfield forming a "computational" leading edge, as illustrated in Fig. 6. In this study the grids are defined such that the physical sharp edge is placed halfway between the computational sharp edge and the two adjacent grid points on the surface. The grid generator, HYGRID, is capable of performing this alteration. Second, a "sharp" boundary condition is implemented in the flow solver, replacing the tangency boundary condition that is used for the rest of the surface points. In the sharp boundary condition, the flow parameters on the computational leading edge are set equal to the values at the points just off the surface; that is, $\rho_{L=1} = \rho_{L=2}$, and similarly for the other conserved variables. This scheme has been used successfully on many test cases including the three solutions presented here.

III. Results

A number of test configurations with known or exact solutions have been used to evaluate the ability of F3D to accurately capture the physics of the waverider flowfields and to test the limitations of the code. The code has an explicit dissipative coefficient used for the central finite differences applied in the η and ζ directions that must be set by the user. In a typical application the dissipation coefficient is slowly reduced from 0.5 to about 0.1 as the solution converges. For Euler test cases up to Mach 4, both the convergence rate and the converged solution appeared to be independent of the dissipative coefficient; that is, identical results were obtained when the coefficient was slowly reduced to 0.1 and when the coefficient remained at 0.5 throughout the convergence. However, for test cases at Mach numbers of 6 or higher, the solutions often became unstable when the dissipation was reduced below 0.5.

For Mach numbers above 2.0, F3D uses a zeroth-order extrapolation to compute the flow density on the surface. Unfortunately, in the Euler solutions there are often gradients normal to the surface that cannot be modeled by the zeroth-order boundary condition, and consequently the accuracy of the solutions is quite sensitive to the grid spacing normal to the wall. As this spacing approaches zero, so does the error associated with the extrapolation. For the test results presented here, wall spacing is typically about 10^{-4} based on a root chord length of 1. The spacing is much tighter at the nose and leading edge, but that limitation is due to the grid generation, not the flow solver.

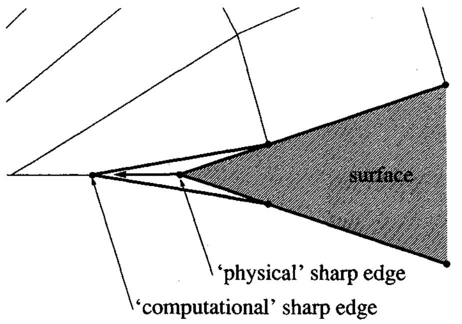

Fig. 6 Grid modifications for the no-point sharp edge.

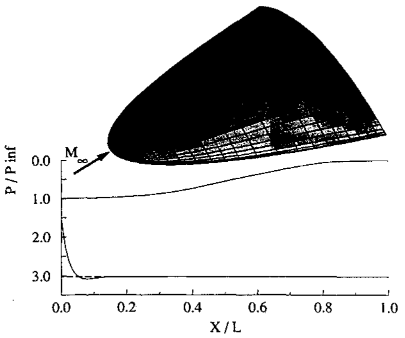

Fig. 7 Planar shock waverider; surface pressure on the symmetry plane: —— F3D Euler simulation, - - - exact solution.

Initial simulations were run without the aid of solution adaptation, using grids with 41 points in the radial or ζ direction. With the addition of solution adaptation, the number of points in the radial direction was reduced to 31, and yet both the surface pressure and shock resolution were more accurately captured.

Sample results for three waverider configurations are presented here. All three generate flowfields that have exact solutions between the shock and the lower surface.

Planar Shock Waverider

The planar shock waverider is similar to the Nonweiler "caret-wing." As its name implies, it produces a planar oblique shock wave resulting in two-dimensional wedge flow between the shock and the lower surface. The surface is analytically defined in this case. The leading edge is defined as a parabola resulting in upper and lower surface cross-sectional profiles that are also parabolic. The upper surface is an expansion surface such that the trailing edge of the configuration is closed. The configuration is designed for Mach 5.5 flow with a shock angle of 17.5 deg. An isometric view of the surface is shown in Fig. 7.

The nondimensional surface pressure along the symmetry plane computed by the F3D Euler solver is compared with the exact, constant value determined by the Rankine-Hugoniot relations in Fig. 7. An exact solution is not known for the upper surface. The shock is smeared over several grid cells at the nose, and a slight pressure overshoot (roughly 7% of the freestream pressure), characteristic of finite difference schemes of order two or higher, is visible just downstream of the shock. Over the remainder of the lower surface the pressure is within 0.01% of the analytic value. Figure 8 compares the nondimensional pressure computed by the Euler solver with the exact solution along a line normal to the lower surface. Again, pressure oscillations are visible on both sides of the shock, but the shock strength and location are captured quite well. Figure 9 shows pressure isolines at a typical cross section on the left half-plane and the exact shock position on the right half-plane. Note that the shock is planar and that it is correctly attached to the leading edge. The shock attachment ideally isolates flows over the upper and lower surfaces of the waveriders as is apparent in Fig. 9. Note that solution-adaptive gridding was not used in this simulation.

Conical Shock Waveriders

Two conical shock waveriders, one designed for Mach 4 and another for Mach 6, have been evaluated. The two config-

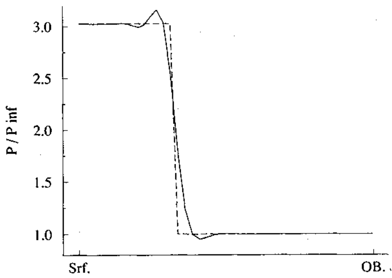

Fig. 8 Planar shock waverider; pressure along a line normal to the lower surface; —— F3D Euler simulation, - - - exact solution.

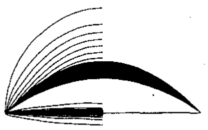

Fig. 9 Planar shock waverider; pressure isolines and exact shock location.

urations were produced at NASA Langley by Bauer et al.[7] using an inverse design and optimization code developed by Bowcutt et al.[8] at the University of Maryland. The algorithm cuts waverider geometries out of known conical flowfields. The conical flowfields are modeled using the Taylor-Maccoll ordinary differential equation, and streamlines defining the lower surface are integrated downstream from a given leading edge using Runge-Kutta integration. The upper surface is allowed to expand but may be constrained for volumetric considerations. The optimization is driven by L/D and is performed by adjusting nine spline parameters that define the leading edge. The optimization includes viscous effects for laminar, transitional, and turbulent boundary layers. Surface pressure distributions predicted by the Bowcutt code can be taken essentially as exact, at least within the bounds of the numerical integration of the Taylor-Maccoll equation for the lower surface and the characteristic solution for the expansion upper surface. The surface definition data output by the Bowcutt code has a rather unusual format with a different number of points defining each cross section, as shown in Fig. 10a. For use in this study the surface data is translated into a more conventional format, shown in Fig. 10b, using cubic-spline interpolation.

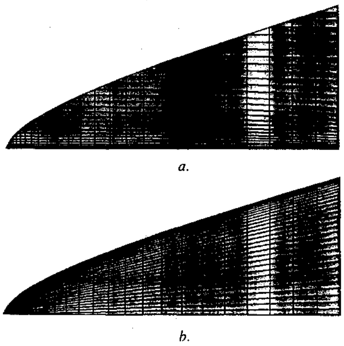

Fig. 10 Surface grids a) output by the Bowcutt code and b) reclustered in this project.

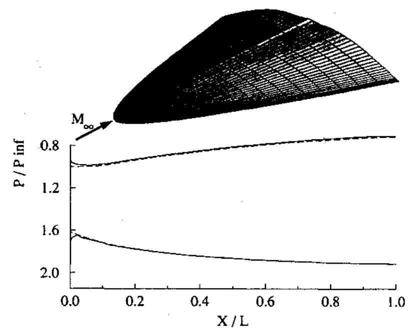

Fig. 11 Mach 4 waverider; surface pressure on the symmetry plane. —— F3D Euler simulation, - - - Bowcutt code.

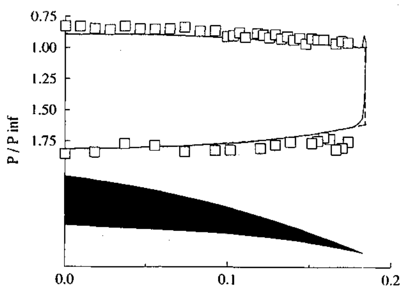

Fig. 12 Mach 4 waverider; surface pressure at 30% root chord: —— F3D Euler simulation, - - - Bowcutt code, □ experimental data.

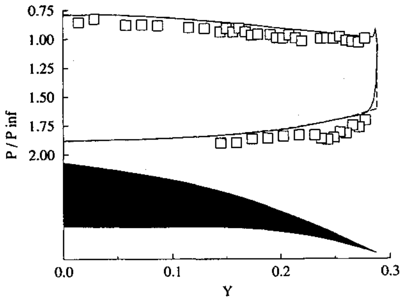

Fig. 13 Mach 4 waverider; surface pressure at 60% root chord: —— F3D Euler simulation, - - - Bowcutt code, □ experimental data.

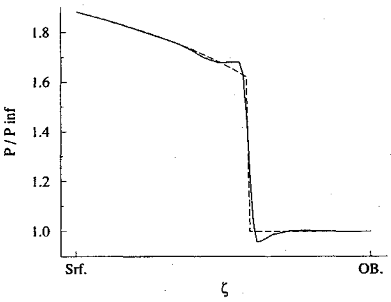

Fig. 14 Mach 4 waverider; pressure along a line normal to the lower surface: —— F3D Euler simulation, - - - Taylor-Maccoll solution.

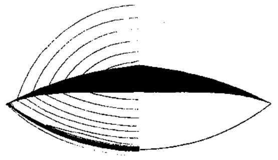

Fig. 15 Mach 4 waverider; pressure isolines and exact shock location.

Table 1 Lift and drag results[a]

Code	M	C_L	C_D	L/D
Bowcutt	4	0.0822	0.00825	9.964
F3D-Euler	4	0.0819	0.00821	9.968
Bowcutt	6	0.0639	0.00739	8.645
F3D-Euler	6	0.0636	0.00731	8.641

[a] Reference area = planform area.

An isometric view of the Mach 4 conical shock waverider is shown in Fig. 11. The configuration is optimized for a fully turbulent boundary layer at a Reynolds number of 5×10^6, based on length, and the base-height-to-length ratio is constrained to 0.087. Figure 11 compares the nondimensional surface pressure predicted by the F3D Euler solver and the Bowcutt code along the symmetry plane. The two methods are in excellent agreement except at the nose where the finite differences of F3D smear the shock. Figures 12 and 13 show nondimensional surface pressure distributions at 30 and 60% of the root chord predicted by F3D and the Bowcutt code compared with experimental data. The values predicted by F3D and the Bowcutt code are in excellent agreement with each other, and the experimental results match reasonably well. The nondimensional pressure predicted by F3D along a line normal to the lower surface is compared with the Taylor-Maccoll solution in Fig. 14. Again, oscillations in the pressure are visible on both sides of the shock, but the shock strength and location are accurately modeled. Figure 15 shows pressure isolines at a typical cross section on the left half-plane and the exact shock position on the right half-plane. Note the conical

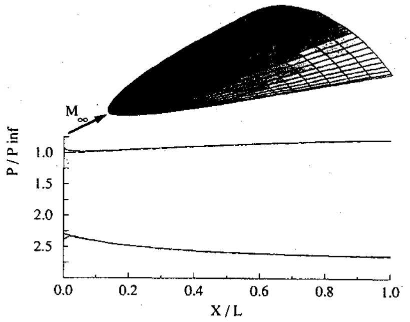

Fig. 16 Mach 6 waverider; surface pressure on the symmetry plane: —— F3D Euler simulation, - - - Bowcutt code.

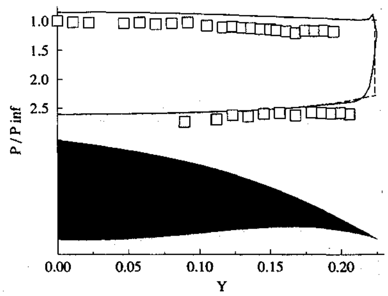

Fig. 17 Mach 6 waverider; surface pressure at 60% root chord: —— F3D Euler simulation, - - - Bowcutt code, □ experimental data.

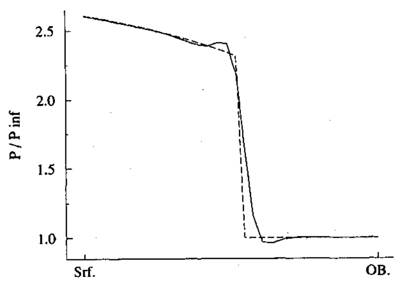

Fig. 18 Mach 6 waverider; pressure along a line normal to the lower surface: —— F3D Euler simulation, - - - Taylor-Maccoll solution.

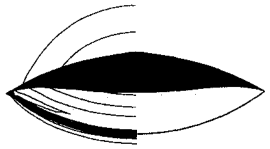

Fig. 19 Mach 6 waverider; pressure isolines and exact shock location.

nature of the flow and the attachment of the shock wave. Lift and drag coefficients computed by both F3D and the Bowcutt code are given in Table 1, and the values are in excellent agreement. Pressure on the base of the model is assumed to be freestream for these calculations. Previous results released by the present authors assumed zero pressure on the base of the model and, therefore, displayed much lower performance characteristics.

The Mach 6 conical shock waverider is optimized for a Reynolds number of 2,666,667, based on length, and a fully turbulent boundary layer. The base-height-to-length ratio is constrained to 0.115. An isometric view of the configuration is shown in Fig. 16 along with a comparison of nondimensional surface pressure along the symmetry plane as predicted by the F3D Euler solver and the Bowcutt code. Again, the two codes are in excellent agreement. Figure 17 compares the nondimensional surface pressure at 60% of the root chord as predicted by F3D and the Bowcutt code with experimental data. Data from the two codes match well, and the experimental data demonstrate a consistent profile. The nondimensional pressure computed by F3D along a line perpendicular to the lower surface is compared with that predicted by the Taylor-Maccoll solution in Fig. 18. The post shock flowfield is captured quite well, but there is a small error in the computed shock position. Figure 19 compares pressure isolines computed by F3D at a typical cross section on the left half-plane with the exact shock position on the right half-plane demonstrating the conical nature of the flowfield and the shock attachment at the sharp leading edge. In this solution, as well as the Mach 4 conical shock waverider, slight deviations from conical flow are visible just behind the shock and near the leading edge. The deviations near the leading edge are primarily due to the spline fitting of surface data for data reclustering, demonstrating the sensitivity of the resultant flowfield to minute changes in surface topology. The deviations elsewhere can generally be reduced by allowing the solution to converge further. However, it was found that further convergence had little or no effect on the computed lift and drag coefficients.

IV. Conclusions

Numerical procedures for the grid generation, solution based grid adaptation, and Euler computation of the inviscid supersonic and hypersonic flowfields around sharp-edged configurations have been developed. A grid generator, HYGRID, with specialized features for adequate handling of sharp leading edges was developed. The ability of the code to produce smooth, well-ordered grids in the vicinity of sharp edges has been demonstrated. An algebraic solution-based grid adaptation technique was developed, and results have illustrated its use. Modifications were made to the F3D flow solver to allow for the computation of stagnation-free flow around sharp leading edges necessary for the capturing of attached shock waves. A number of test configurations have been studied to evaluate the ability of these procedures to accurately capture the physics of these flowfields. Results from three waverider simulations have been compared with exact theory, other numerical procedures, and experimental data. Comparisons indicate excellent agreement between the F3D Euler solutions, exact theory, and results from the Bowcutt code, and the results match available experimental data reasonably well. An investigation of the sensitivity of the Euler solver to variations in the dissipation coefficients has indicated that relatively high dissipation may be used throughout the solution convergence without noticeable solution degradation, whereas the use of low dissipation at high Mach numbers often leads to instability. Due to the zeroth-order surface density boundary condition applied at Mach numbers over 2, the computed surface pressure and, hence, the lift and drag results were found to be quite sensitive to the grid spacing normal to the surface. This study has highlighted a few weaknesses in the procedures but has nonetheless demonstrated the ability of the codes to model these waverider flowfields with sufficient accuracy.

Acknowledgments

This work was supported by NASA Langley through Contract NAG-1-880. Computer resources were provided by NASA Langley and the University of Colorado. Additional support was provided by the DLR in Göttingen, Germany, and by the University of Colorado. The authors would like to give special thanks to Steven Bauer of the Supersonic/Hypersonic Aerodynamics Branch (SHAB) at NASA Langley for the experimental data presented here.

References

[1]Nonweiler, T. R. F., "Aerodynamic Problems of Manned Space Vehicles," *Journal of the Royal Aeronautical Society,* Vol. 63, 1959, pp. 521-528.

[2]Jones, J. G., "A Method for Designing Lifting Configurations for High Supersonic Speeds Using the Flow Fields of Non-Lifting Cones," Royal Aircraft Establishment, Rept. Aero. 2674, Bedford, England, U.K., March 1963.

[3]Sobieczky, H., Dougherty, F. C., and Jones, K. D., "Hypersonic Waverider Design from Given Shock Waves, *Proceedings of the 1st International Hypersonic Waverider Symposium,* Univ. of Maryland, College Park, MD, Oct. 17-19, 1990.

[4]Rizzi, A., and Eriksson, L. E., "Transfinite Mesh Generation and Damped Euler Equation Algorithm for Transonic Flow Around Wing-Body Configurations," AIAA Paper 81-0999, June 1981.

[5]Pulliam, T. H., "Euler and Thin Layer Navier-Stokes Codes: ARC2D, ARC3D," *Notes for Computational Fluid Dynamics User's Workshop,* Univ. of Tennessee Space Inst., UTSI Publication E02-4005-023-84, Tullahoma, TN, March 1984.

[6]Ying, S. X., Steger, J. L., Schiff, L. B., and Bagandoff, D., "Numerical Simulation of Unsteady, Viscous, High-Angle-of-Attack Flows Using a Partially Flux-Split Algorithm," AIAA Paper 86-2179, Aug. 1986.

[7]Bauer, S. X. S., Covell, P. F., Forrest, D. K., and McGrath, B. E., "Preliminary Assessment of a Mach 4 and a Mach 6 Waverider," *Proceedings of the 1st International Hypersonic Waverider Symposium,* Univ. of Maryland, College Park, MD, Oct. 17-19, 1990.

[8]Bowcutt, K. G., Anderson, J. D., and Capriotti, D., "Viscous Optimized Hypersonic Waveriders," AIAA Paper 87-0272, Jan. 1987.

Gerald T. Chrusciel
Associate Editor

MANUSCRIPT DISKS TO BECOME MANDATORY

As of January 1, 1993, authors of all journal papers prepared with a word-processing program must submit a computer disk along with their final manuscript. AIAA now has equipment that can convert virtually any disk (3½-, 5¼-, or 8-inch) directly to type, thus avoiding rekeyboarding and subsequent introduction of errors.

Please retain the disk until the review process has been completed and final revisions have been incorporated in your paper. Then send the Associate Editor all of the following:

- Your final version of the double-spaced hard copy.
- Original artwork.
- A copy of the revised disk (with software identified).

Retain the original disk.

If your revised paper is accepted for publication, the Associate Editor will send the entire package just described to the AIAA Editorial Department for copy editing and typesetting.

Please note that your paper may be typeset in the traditional manner if problems arise during the conversion. A problem may be caused, for instance, by using a "program within a program" (e.g., special mathematical enhancements to word-processing programs). That potential problem may be avoided if you specifically identify the enhancement and the word-processing program.

The following are examples of easily converted software programs:

- PC or Macintosh TEX and LATEX
- PC or Macintosh Microsoft Word
- PC Wordstar Professional

If you have any questions or need further information on disk conversion, please telephone Richard Gaskin, AIAA Production Manager, at 202/646-7496.

AIAA
American Institute of
Aeronautics and Astronautics